

Multiband superconductivity in $\text{Ta}_4\text{Pd}_3\text{Te}_{16}$ with anisotropic gap structure

Wen-He Jiao,^{1,*} Yi Liu,² Yu-Ke Li,³ Xiao-Feng Xu,³ Jin-Ke Bao,²
Chun-Mu Feng,² S. Y. Li,^{4,5} Zhu-An Xu,^{2,5} and Guang-Han Cao^{2,5,†}

¹*School of Science, Zhejiang University of Science and Technology, Hangzhou 310023, China*

²*Department of Physics, Zhejiang University, Hangzhou 310027, China*

³*Department of Physics, Hangzhou Normal University, Hangzhou 310036, China*

⁴*State Key Laboratory of Surface Physics, Department of Physics,*

and Laboratory of Advanced Materials, Fudan University, Shanghai 200433, China

⁵*Collaborative Innovation Centre of Advanced Microstructures, Nanjing University, Nanjing 210093, China*

(Dated: March 24, 2021)

We carried out the measurements of magnetoresistance, magnetic susceptibility and specific heat on crystals of the low-dimensional transition metal telluride $\text{Ta}_4\text{Pd}_3\text{Te}_{16}$. Our results indicate that $\text{Ta}_4\text{Pd}_3\text{Te}_{16}$ is an anisotropic type-II superconductor with the extracted Ginzburg-Landau parameter $\kappa_{\text{GL}} = 84$. The upper critical field $H_{c2}(T)$ shows a linear dependence at low temperature and the anisotropy of $H_{c2}(T)$ is strongly T -dependent, both of which indicate a multiband scenario. A detailed analysis reveals that the electronic specific heat $C_{\text{el}}(T)$ can be consistently described by a two-gap ($s+d$ waves) model from the base temperature $T/T_c \sim 0.12$ up to T_c . Our data suggests multiband superconductivity in $\text{Ta}_4\text{Pd}_3\text{Te}_{16}$ with anisotropic gap structure.

PACS numbers: 74.70.-b, 74.78.-w, 74.25.Op, 74.25.Bt

Exploring exotic pairing mechanisms in new superconducting compounds have always been one of the most attractive issues in condensed matter physics. Although the Bardeen-Cooper-Schrieffer (BCS) theory¹ provides excellent explanations for the conventional phonon-mediated s -wave superconductor, the successive emergence of unconventional superconductivity, claimed to be in either the singlet s_{\pm} -wave² and d -wave pairing states,^{3,4} or the triplet p -wave^{5,6} and f -wave pairing states,⁷ presents great challenges for physicists to uncover the variously exotic non-phonon-mediated pairing mechanisms. The spin or charge fluctuations, which always appear in low-dimensional structures, were often regarded as the pairing glues for a large number of unconventional superconductors, such as the cuprates,⁸ iron-based superconductors,² quasi-one-dimensional (Q1D) superconductors,^{9,10} and heavy-fermion superconductors.^{11,12} Among them, multiband superconductivity and symmetry-imposed nodes were commonly observed as evidenced by a variety of techniques including thermodynamic approaches.^{13–15} In this regard, the gained information on the gap symmetry has significant meanings in understanding the novel pairing mechanisms.

Recently, we discovered bulk superconductivity with $T_c = 4.6$ K in a transition metal telluride $\text{Ta}_4\text{Pd}_3\text{Te}_{16}$.¹⁶ This material has a layered structure with Q1D characteristics consisting of PdTe_2 chains, TaTe_3 chains and Ta_2Te_4 double chains along the crystallographic b -axis. The (103) planes, as illustrated in the inset of Fig. 1(c), are formed by the connection of the chains mentioned above along the $[301]$ direction. These structural features are well reflected in the morphology of the crystals as shown in the inset of Fig. 1(a). For simplicity, hereafter we define a^* -axis as to be parallel to the $[301]$ direction and c^* -axis as to be perpendicular to

the $(\bar{1}03)$ plane. Compared with layered chalcogenide superconductors $\text{Nb}_3\text{Pd}_x\text{Se}_7$ ¹⁷ and $M_2\text{Pd}_x\text{Q}_5$ ($M = \text{Nb}$ and Ta , $Q = \text{S}$ and Se)^{18–21} with similar Q1D structures, $\text{Ta}_4\text{Pd}_3\text{Te}_{16}$ is a stoichiometric compound with flat two-dimensional sheets and it shows stronger electron-electron interactions.¹⁶ Thermal conductivity measurements demonstrate the presence of nodes in the superconducting gap by the evidences of a large residual κ_0/T in zero field and the rapid increase of κ_0/T in magnetic field, mimicking the behavior of d -wave cuprate superconductor Tl-2201.²² Furthermore, a temperature-pressure superconducting dome was as well observed, leading to the expectation that certain density-wave orders may neighbour the superconducting dome. According to the result of electronic structure calculations made by Singh,²³ any nearby density wave instability, if exists, would be a charge-density-wave (CDW) but not a spin-density-wave (SDW) as the transition metal contribution to the density of states is rather small. Besides, an s -wave pairing state from phonons associated with the Te-Te p bonding and a Fermi surface associated Te p bands are argued to be the most possible case. To explain the results of the thermal conductivity, the author also proposes the likelihood of $\text{Ta}_4\text{Pd}_3\text{Te}_{16}$ being a clean multi-gap superconductor where the gap ratio is significantly large.²³ However, more recently, the low-temperature scanning tunneling spectroscopy (STS) measurements show the evidence for the presences of anisotropic superconducting gap with gap minima or even node.²⁴ Thus, the issue of the gap symmetry in $\text{Ta}_4\text{Pd}_3\text{Te}_{16}$ is worthy to be addressed further.

In this Rapid Communication, we investigate the superconducting properties of the $\text{Ta}_4\text{Pd}_3\text{Te}_{16}$ crystals via systematic magnetoresistivity (MR), magnetic susceptibility and specific heat measurements. The

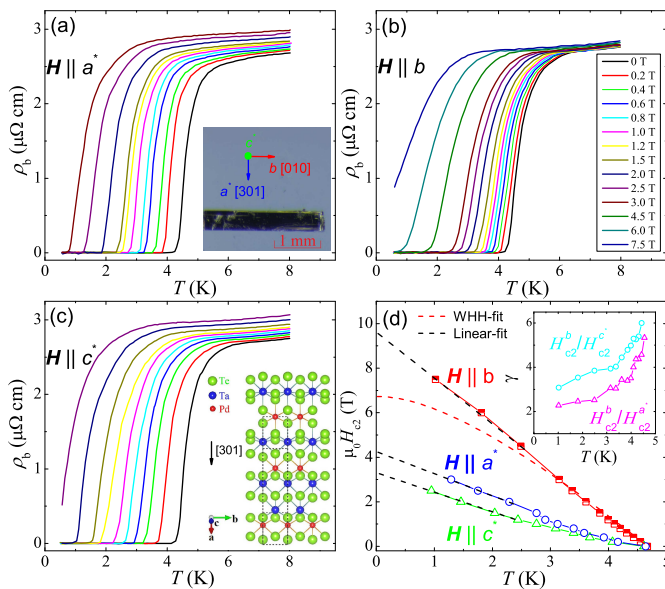


FIG. 1. (Color online) Magnetoconductivity of the Ta₄Pd₃Te₁₆ crystal for (a) $H \parallel a^*$, (b) $H \parallel b$ and (c) $H \parallel c^*$. (d) The extracted superconducting upper critical field $H_{c2}(T)$ for different field orientations. Werthamer-Helfand-Hohenberg (WHH) fitting is made to the data for $H \parallel b$, represented by the red dashed lines. The black dashed lines show linear fittings. The inset of (a) shows the image of the crystal under an optical microscope, from which the crystallographic directions can be easily identified. The crystal structure of Ta₄Pd₃Te₁₆ viewed perpendicular to the $(\bar{1}03)$ plane is plotted in the inset of (c). The inset of (d) shows the anisotropy of $H_{c2}(T)$.

results indicate that Ta₄Pd₃Te₁₆ is an anisotropic type-II superconductor. The upper critical fields $H_{c2}(0)$ were estimated to be 4.2, 9.6 and 3.3 T for fields applied along the three axes, a^* , b and c^* , respectively. We observed strong T -dependent anisotropy of $H_{c2}(T)$ and the linear increase H_{c2} , both of which suggest the multiband superconductivity. The zero-field heat capacity data can be best described by a two-gap model with anisotropic gap structure. In addition, the electronic specific heat coefficient in the mixed state, $\gamma_e(H)$, exhibits a nonlinear behavior. Thus, our results suggest two energy gaps with anisotropic gap structure are associated with the superconductivity in Ta₄Pd₃Te₁₆.

Single crystals of Ta₄Pd₃Te₁₆ were grown by a self-flux technique as previously described.¹⁶ High quality of as-grown crystals was confirmed by X-ray diffraction. To insure the data obtained more reliable, we elaborately selected crystals for the measurements, all of which having shiny surfaces without any discernible solvent attached. MR measurements were carried out by a stand four-probe technique with current $I = 2$ mA applied along the b -axis. The specific heat for a collection of five needle-like crystals with a total mass $m = 4.68(2)$ mg was measured by a long relaxation method utilizing a commercial ³He microcalorimeter (Quantum Design PPMS-9). In various magnetic fields, the thermometer on the calorimeter puck was calibrated before the measurements, and the addenda was predetermined in a separate run. Magnetic susceptibility measurement was performed using a superconducting quantum interference device magnetometer (MPMS-5).

Figure 1 encapsulates the b -axis MR (ρ_b) and the extracted H_{c2} with fields applied along a^* , b and c^* , respectively. To eliminate the ambiguity from the superconducting fluctuations, the 50% criterion was used in determining H_{c2} , *i.e.*, the field at which ρ_b reaches 50% of the normal state resistivity. We employed the Werthamer-Helfand-Hohenberg (WHH) formula for an isotropic one-band BCS superconductor in a dirty limit to fit $H_{c2}^b(T)$.²⁵ Apparently, at low temperatures, the one-band WHH model fails to satisfy the extracted $H_{c2}^b(T)$. By linear extrapolations, H_{c2}^{a*} , $H_{c2}^b(T)$ and H_{c2}^c are estimated to be 4.2, 9.6 and 3.3 T, respectively. The estimated value of $H_{c2}^b(T)$ is close to the Pauli-Clogston limiting field $H_p = 1.84T_c \sim 8.5$ T, excluding the possibility of triplet pairing. Besides, all of the three curves show a linear T -dependence at low temperatures, which is consistent with the previous report²² but in sharp contrast with what it should display in most superconductors,^{25,26} *i.e.*, a concave down curvature at low temperatures. This anomalous behavior was regarded as the evidence for multiband superconductivity in iron-based superconductors.^{27,28} Moreover, as shown in the inset of Fig. 1(d), the strong T -dependent superconducting anisotropy $\gamma = H_{c2}^b/H_{c2}^{c*}$ or H_{c2}^b/H_{c2}^{a*} provides further evidence for multiband scenario as the case in two-band superconductor MgB₂ and most iron-based superconductors.^{29,30} Using the anisotropic GL formula

$$H_{c2}^i(0) = \phi_0/2\pi\xi_j(0)\xi_k(0), \quad (1)$$

where ϕ_0 is the flux quantum and $\xi_j(0)$ is the GL

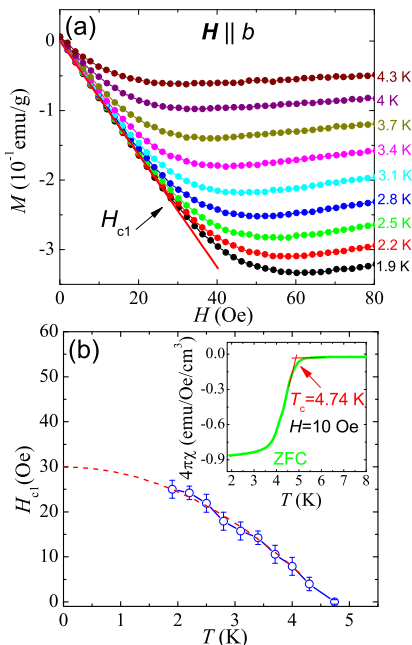


FIG. 2. (Color online) (a) The low-field magnetization curve $M(H)$ under field applied along b -axis at various temperatures. The solid red line is fitted to the 1.9 K data. (b) The extracted $H_{c1}^b(T)$ for $\text{Ta}_4\text{Pd}_3\text{Te}_{16}$. The inset shows the diamagnetic signal under 10 Oe with zero-field-cooling (ZFC) mode.

coherence length along the j -direction, $\xi(0)$ at zero temperature is calculated to be 66.1, 151.0 and 51.9 Å for a^* , b and c^* , respectively. Obviously, the interchain coherence lengths $\xi^{a^*}(0)$ and $\xi^{c^*}(0)$ are much longer than the distance between any two adjacent chains in $\text{Ta}_4\text{Pd}_3\text{Te}_{16}$ denoting the continuous superconducting phase across the chains. In other words, the superconductivity here is anisotropic but three-dimensional in nature, similar to recent discovered Q1D superconductors $\text{Nb}_2\text{Pd}_x\text{Se}_5$ and $\text{Ta}_2\text{Pd}_x\text{S}_5$.^{19,20} For the normal state, the longitudinal MR ($\mathbf{H} \parallel \mathbf{I}$) response is negligibly small, while the in-chain MR ($\mathbf{H} \perp \mathbf{I}$) is obviously large in magnitude and positive, which is typical of a Q1D metal due to the change in carrier trajectories induced by the Lorentz force.³¹

The lower critical field values, $H_{c1}^b(T)$, were determined from low-field magnetization curves $M(H)$ with field applied along the b -axis as shown in Fig. 2. The low-field parts almost overlap with the Meissner line (the solid red line in Fig. 2(a)) due to the Meissner effect. Thus, $H_{c1}^b(T)$ could be defined at the point where $M(H)$ deviate by 2% from the perfect Meissner response, and the extracted results are plotted in Fig. 2(b). Since that our crystal is needle-like and the demagnetization factor for field along the needle-like direction is negligibly small, $H_{c1}^b(0)$ can be directly estimated to be 29.9 Oe by fitting the extracted data to the formula, $H_{c1}^b(T) = H_{c1}^b(0)[1 - (T/T_c)^2]$, represented by the dashed red line in Fig. 2(b). With the results for $H_{c1}^b(0)$ and $H_{c2}^b(0)$, we

calculated the GL parameter κ_{GL}^b to be about 84 using the equation $H_{c2}(0)/H_{c1}(0) = 2\kappa_{\text{GL}}^2/\ln\kappa_{\text{GL}}$. The above results indicate that $\text{Ta}_4\text{Pd}_3\text{Te}_{16}$ is an extremely type-II superconductor.

Figure 3 presents the T -dependent specific heat of $\text{Ta}_4\text{Pd}_3\text{Te}_{16}$ crystals divided by temperature at zero magnetic field. A sharp anomaly, denoting the superconducting transition, can be clearly observed at $T_c \sim 4.14$ K (defined by an entropy conserving construction). In Fig. 3(a), the raw heat capacity data between 3.5 K and 7 K is fitted to the formula $C/T = \gamma + \beta T^2$, and the fitting gives parameters $\gamma = 51.2(1)$ mJ/mol K² and $\beta = 13.53(1)$ mJ/mol K⁴, both of which are slightly larger than our previous report.¹⁶ This small discrepancy is possibly due to the measurement precision as well as the uncertainty of sample mass weighed. Besides, a small residual linear term $\gamma_0 = 5.1$ mJ/mol K² exists, as observed from the intercept of C/T vs T^2 in the $T \rightarrow 0$ limit, the origin of which may be the presence of nodal quasiparticles for a nodal superconducting gap or a small fraction of nonsuperconducting metallic impurity phase. By subtracting the phononic contribution, the electronic specific heat can be obtained by: $C_{\text{el}}(T) = C(T) - \beta T^3$, which is plotted in Fig. 3(b) as C_{el}/T versus T/T_c . The zero-field data at low temperature is obviously irreconcilable with the conventional s -wave order parameter as the significant quasi-particle excitations.

The so-called α model, which was devised to simulate the strong-coupling effect, has gained significant success in explaining the properties of strong-coupling superconductors.³² Within this model, the temperature dependence of energy gap $\Delta(T)$ approximately follows weak-coupling BCS behavior multiplied by a dimensionless parameter α . In the BCS theory, the entropy S in the superconducting state is given by³³

$$S = -\frac{3\gamma_n}{k_B\pi^3} \int_0^{2\pi} \int_0^\infty f \ln f + [1-f] \ln [1-f] d\varepsilon d\phi, \quad (2)$$

where f is the Fermi function $f = (1 + e^{E/k_B T})^{-1}$ with the quasiparticle energy $E = \sqrt{\varepsilon^2 + \Delta^2(T, \phi)}$, γ_n is the normal state γ for the superconducting part, and $\Delta(T, \phi)$ is the temperature and angle dependence of the gap function. The electronic heat capacity is thus calculated by $C_{\text{el}} = T(\partial S/\partial T)$. To elucidate the superconducting order parameter, the raw data of C_{el} is analyzed and fitted by various models, *i.e.*, the isotropic s -wave function, anisotropic d -wave function, two-fold-symmetric anisotropic s -wave function [$\Delta(\phi) = \alpha_1 + \alpha_2 \cos 2\phi$], and two-gap scenarios ($s+s$ waves and $s+d$ waves). The contribution of C_{el} from nodal quasiparticles or the small fraction of nonsuperconducting metallic impurity phase is regarded as $\gamma_0 T$ in our fittings. The fitting curves for the cases of single-band d -wave and two-band $s+d$ waves are plotted in Fig. 3(b), from which, one can unambiguously observe that the two-gap ($s+d$ waves) model best captures the experimental data from the base temperature $T/T_c \sim 0.12$ up to T_c . The fitting

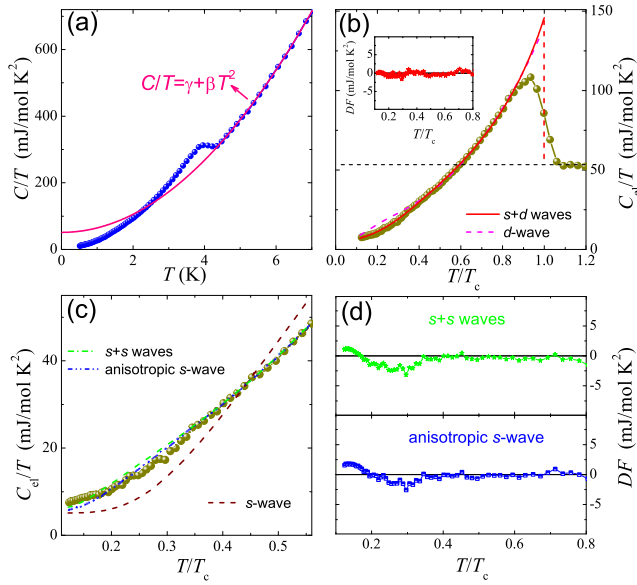


FIG. 3. (Color online) (a) Specific heat of $\text{Ta}_4\text{Pd}_3\text{Te}_{16}$ crystals divided by temperature (C/T) at zero magnetic field. The solid pink line is the fit to the normal-state data from 4.5 to 7 K using the formula $C/T = \gamma + \beta T^2$. (b) T -dependent electronic contribution to the specific heat divided by temperature (C_{e1}/T). Red and magenta dashed lines are the fitting curves with two-gap ($s+d$ waves) and single-gap d -wave scenarios. The inset shows the deviation of the fitting value for the case of $s+d$ waves with the data (represented by DF in the plot). (c) expands the low temperature region. Lines show the theoretical fitting of various s -wave gap functions as described in the text. (d) The deviation of the fitting from the data for the cases of $s+s$ waves (upper panel) and anisotropic s -wave (lower panel).

gives the following parameters: $\alpha^s = 0.916$ (for s wave), $\alpha^d = 1.652$ (for d wave) and the ratio of weight $\gamma_n^s : \gamma_n^d = 33.5 : 66.5$, where the partial Sommerfeld coefficient $\gamma_n^{s(d)}$ characterizes each band. Nodal quasiparticles for the nodal superconducting gap or impure phase are expected to be the source of the finite value γ_0 in $T \rightarrow 0$ limit for this case. The fittings with other gap functions (full-gap cases) mentioned above deviate the experimental data significantly, especially in low-temperature region, the close-up view of which is displayed in Fig. 3(c). For the full-gap cases, the residual linear term γ_0 should come from a small amount of nonsuperconducting metallic impure phase. In order to show more clearly the deviations of the fitting curves from the data for the case of $s+s$ waves and anisotropic s -wave, we plots the differences in Fig. 3(d). Therefore, our result strongly suggests $\text{Ta}_4\text{Pd}_3\text{Te}_{16}$ is a two-gap superconductor with the pairing symmetry of $s+d$ waves. This fitting is consistent with the STS study as the temperature dependence of tunneling spectra can be well fitted with $s+d$ waves (the anisotropic s -wave symmetry can as well describe their data while in our heat-capacity study it can not).²⁴ In addition, by calculating the maximum gap

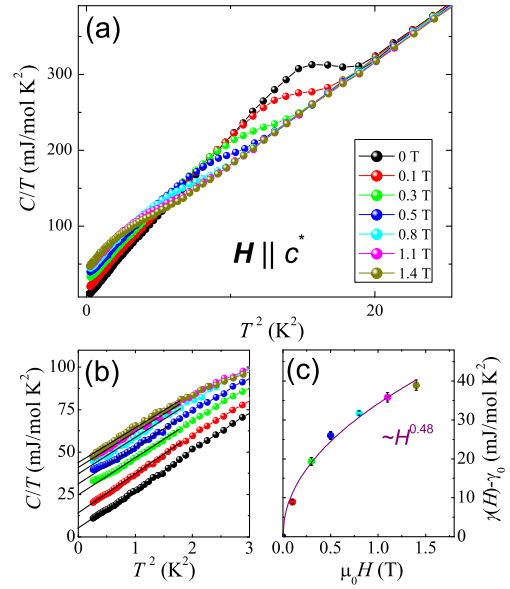


FIG. 4. (Color online) (a) Specific heat of $\text{Ta}_4\text{Pd}_3\text{Te}_{16}$ crystals in selected magnetic fields parallel to c^* -axis, plotted as C/T vs T^2 . (b) The plots of C/T vs T^2 in the low- T region. For each applied field, $\gamma(H) \equiv \lim_{T \rightarrow 0} C(T, H)/T$ was determined from a linear extrapolation of the experimental data in the temperature range 0.5–1.3 K. (c) Magnetic field dependence of the electronic specific heat coefficient $\gamma(H)$ in the mixed state.

value using the derived parameters ($\Delta_{\max} = 0.335 \cdot \Delta^s + 0.665 \cdot \Delta^d$), we find that $\Delta_{\max}/k_B T_c \approx 2.47$, very close to the value 2.3 reported in Ref. 24. The scenario of two-band s -wave gaps with significant ratio has been proposed to be possible in understanding the data of thermal conductivity.²³ However, our analysis of the heat capacity does not provide sufficient evidence for this possibility. On the contrary, the evidence of anisotropic multi-gap structure is consistent with the study of thermal conductivity,²² which suggests the presence of node in the superconducting gap. Overall, our result reported here reconciles the recent experimental studies regarding the pairing symmetry in $\text{Ta}_4\text{Pd}_3\text{Te}_{16}$.

As the magnetic field dependence of specific heat at low temperatures is instructive for the quasi-particle excitations, we measured the low- T specific heat of $\text{Ta}_4\text{Pd}_3\text{Te}_{16}$ crystals under magnetic fields ($\mu_0 H \leq 1.4$ T) for $\mathbf{H} \parallel c^*$ as shown in Fig. 4(a). The heat capacity anomaly is gradually suppressed to lower temperatures with the increase of field. The enlarged part of the data is displayed in Fig. 4(b), from which, one can observe that minor upturns under $\mu_0 H = 0.3$ and 0.5 T appear at low temperatures, probably stemming from Schottky anomaly. Therefore, we extracted field-dependent electronic coefficient $\gamma(H)$ by a linear extrapolation of $\gamma(H) \equiv \lim_{T \rightarrow 0} C(T, H)/T$, without considering the upturns under 0.3 and 0.5 T. The obtained results are presented in Fig. 4(c) as $\gamma_e(H) = \gamma(H) - \gamma_0$ vs H . In fully gapped conventional type-

II superconductors, it is generally known that $\gamma_e(H)$ should be linearly proportional to the number of field-induced vortices,³⁴ *i.e.*, $\gamma_e(H) \propto H$. However, we find in Ta₄Pd₃Te₁₆, a power-law fitting provides the relation $\gamma_e(H) \sim H^{0.48}$ as shown in Fig. 4(c), thereby ruling out the isotropic *s*-wave pairing symmetry. In the case of two isotropic *s*-wave superconducting gaps, $\gamma_e(H)$ is featured by an intersection of two straight lines, as observed in multiband superconductivity with two *s*-wave gaps, *e.g.*, MgB₂,³⁵ NbSe₂,³⁶ and SrPt₂As₂.³⁷ The nonlinear behavior observed here is seemingly in contrast with the above scenario. Although \sqrt{H} behavior was once considered as the evidence of *d*-wave superconductors due to the Doppler shift of extended quasi-particle excitation spectrum,³⁸ this kind of nonlinear behavior was also frequently observed in many multiband superconductors, such as TlNi₂Se₂.¹⁵ Overall, the nonlinear behavior for $\gamma_e(H)$ could be regarded as an evidence for multiband superconductivity.

In summary, we have investigated the superconducting properties of Ta₄Pd₃Te₁₆ crystals. Our measurements indicate Ta₄Pd₃Te₁₆ is a new anisotropic type-II superconductor with the extracted Ginzburg-Landau

parameter $\kappa_{GL} = 84$. The linear *T*-dependent H_{c2} at low temperatures and the strong *T*-dependent anisotropy of H_{c2} suggest the multiband superconductivity. Indeed, the zero-field electronic heat capacity data, C_{el} , can be satisfactorily described in terms of a two-gap (*s+d* waves) model. The electronic heat capacity coefficient, $\gamma_e(H)$, exhibiting a nonlinear behavior. Thus, Ta₄Pd₃Te₁₆ appears to be a rare example of a two-gap superconductor with the gap symmetry of *s+d* waves rather than a multiple fully gapped *s*-wave symmetry. This superconducting state is very interesting and worthy to investigate further, especially when noting the Q1D structural characteristics in Ta₄Pd₃Te₁₆.

ACKNOWLEDGMENTS

We would like to thank Huiqiu Yuan and Yongkang Luo for helpful discussions. This work is supported by National Basic Research Program of China (Nos. 2011CBA00103 and 2010CB923003) and National Science Foundation of China (No. 11190023).

* whjiao@zust.edu.cn

† ghcao@zju.edu.cn

¹ J. Bardeen, L. N. Cooper, and J. R. Schrieffer, Phys. Rev. **108**, 1175 (1957).

² P. J. Hirschfeld, M. M. Korshunov, and I. I. Mazin, Rep. Prog. Phys. **74**, 124508 (2011).

³ C. C. Tsuei and J. R. Kirtley, Rev. Mod. Phys. **72**, 969-1016 (2000).

⁴ K. An, T. Sakakibara, R. Settai, Y. Onuki, M. Hiragi, M. Ichioka, and K. Machida, Phys. Rev. Lett. **104**, 037002 (2010).

⁵ A. P. Mackenzie and Y. Maeno, Rev. Mod. Phys. **75**, 657 (2000).

⁶ X. F. Xu, A. F. Bangura, J. G. Analytis, J. D. Fletcher, M. M. J. French, N. Shannon, J. He, S. Zhang, D. Mandrus, R. Jin, and N. E. Hussey, Phys. Rev. Lett. **102**, 206602 (2009).

⁷ I. I. Mazin and M. D. Johannes, Nature Phys. **1**, 91 (2005).

⁸ P. A. Lee, N. Nagaosa, and X. G. Wen, Rev. Mod. Phys. **78**, 17 (2006).

⁹ Y. Tanaka, Y. Yanase, and M. Ogata, J. Phys. Soc. Jpn. **73**, 2053 (2004).

¹⁰ K. Kuroki and Y. Tanaka, J. Phys. Soc. Jpn. **74**, 1694 (2005).

¹¹ N. D. Mathur, F. M. Grosche, S. R. Julian, I. R. Walker, D. M. Freye, R. K. W. Haselwimmer, and G. G. Lonzarich, Nature **394**, 39 (1998).

¹² M. Jourdan, M. Huth, and H. Adrian, Nature **398**, 47 (1999).

¹³ G. Mu, H. Q. Luo, Z. S. Wang, L. Shan, C. Ren, and H. H. Wen, Phys. Rev. B **79**, 174501 (2009).

¹⁴ J. Hu, T. J. Liu, B. Qian, A. Rotaru, L. Spinu, and Z. Q. Mao, Phys. Rev. B **83**, 134521 (2011).

¹⁵ H. D. Wang, C. H. Dong, Q. H. Mao, R. Khan, X. Zhou,

C. X. Li, B. Chen, J. H. Yang, Q. P. Su, and M. H. Fang, Phys. Rev. Lett. **111**, 207001 (2013).

¹⁶ W. H. Jiao, Z. T. Tang, Y. L. Sun, Y. Liu, Q. Tao, C. M. Feng, Y. W. Zeng, Z. A. Xu, and G. H. Cao, J. Am. Chem. Soc. **136**, 1284 (2014).

¹⁷ Q. R. Zhang, D. Rhodes, B. Zeng, T. Besara, T. Siegrist, M. D. Johannes, and L. Balicas, Phys. Rev. B **88**, 024508 (2013).

¹⁸ Q. Zhang, G. Li, D. Rhodes, A. Kiswandhi, T. Besara, B. Zeng, J. Sun, T. Siegrist, M. D. Johannes, L. Balicas, Sci. Rep. **3**, 1446 (2013).

¹⁹ S. Khim, B. Lee, K. Y. Choi, B. G. Jeon, D. H. Jang, D. Patil, S. Patil, R. Kim, E. S. Choi, S. Lee, J. Yu, and K. H. Kim, New J. Phys. **15**, 123031 (2013).

²⁰ Y. F. Lu, T. Takayama, A. F. Bangura, Y. Katsura, D. Hashizeme, and H. Takagi, J. Phys. Soc. Jpn. **83**, 023702 (2014).

²¹ N. Zhou, X. F. Xu, J. R. Wang, J. H. Yang, Y. K. Li, Y. Guo, W. Z. Yang, C. Q. Niu, B. Chen, C. Cao, and J. H. Dai, Phys. Rev. B **90**, 094520 (2014).

²² J. Pan, W. H. Jiao, X. C. Hong, Z. Zhang, L. P. He, P. L. Cai, J. Zhang, G. H. Cao, and S. Y. Li, arXiv: 1404.0371 (2014).

²³ D. J. Singh, Phys. Rev. B **90**, 144501 (2014).

²⁴ Z. Y. Du, D. I. Fang, Z. Y. Wang, Y. F. Li, G. Du, H. Yang, X. Y. Zhu, and H. H. Wen, arXiv: 1412.3993 (2014).

²⁵ N. R. Werthamer, E. Helfand, and P. C. Hohenberg, Phys. Rev. **147**, 295 (1966).

²⁶ M. Tinkham, Introduction to Superconductivity (McGraw-Hill, New York, 1975).

²⁷ H. Q. Yuan, J. Singleton, F. F. Balakirev, S. A. Baily, G. F. Chen, J. L. Luo, and N. L. Wang, Nature (London) **457**, 565 (2009).

²⁸ S. Khim, B. Lee, J. W. Kim, E. S. Choi, G. R. Stewart,

- and K. H. Kim, Phys. Rev. B **84**, 104502 (2011).
- ²⁹ M. Angst, R. Puzniak, A. Wisniewski, J. Jun, S. M. Kazakov, J. Karpinski, J. Roos, and H. Keller, Phys. Rev. Lett. **88**, 167004 (2002).
- ³⁰ D. C. Johnston, Adv. Phys. **59**, 803 (2010).
- ³¹ I. Terasaki, N. Seiji, S. Adachi, and H. Yamauchi, Phys. Rev. B **54**, 11993 (1996).
- ³² H. Padamsee, J. E. Neighbor, and C. A. Shiffman, J. Low Temp. Phys. **12**, 387 (1973).
- ³³ F. Bouquet, Y. Wang, R. A. Fisher, D. G. Hinks, J. D. Jorgensen, A. Junod, and N. E. Phillips, Europhys. Lett. **56**, 856 (2001).
- ³⁴ C. Caroli, P. G. Gennes, and J. Matricon, Phys. Lett. **9**, 307 (1964).
- ³⁵ F. Bouquet, Y. Wang, I. Sheikin, T. Plackowski, A. Junod, S. Lee, and S. Tajima, Phys. Rev. Lett. **89**, 257001 (2002).
- ³⁶ E. Boaknin, M. A. Tanatar, J. Paglione, D. Hawthorn, F. Ronning, R. W. Hill, M. Sutherland, L. Taillefer, J. Sonier, S. M. Hayden, and J. W. Brill, Phys. Rev. Lett. **90**, 117003 (2003).
- ³⁷ X. F. Xu, B. Chen, W. H. Jiao, B. Chen, C. Q. Niu, Y. K. Li, J. H. Yang, A. F. Bangura, Q. L. Ye, C. Cao, J. H. Dai, G. H. Cao, and N. E. Hussey, Phys. Rev. B **87**, 224507 (2013).
- ³⁸ G. E. Volovik, JETP Lett. **58**, 469 (1993).